

# **Innovative system of very wide field optical sensors for space surveillance in the LEO region**

**L. Dimare, D. Farnocchia, G. F. Gronchi, A. Milani, F. Bernardi**

*Department of Mathematics, University of Pisa, Largo B. Pontecorvo, 5, 56127, Pisa, Italy*

**Alessandro Rossi**

*IFAC-CNR & ISTI-CNR, via Madonna del Piano 10, 50019, Sesto Fiorentino (FI), Italy*

## **ABSTRACT**

We present the results of a large scale simulation, reproducing the behavior of a data center for the build-up and maintenance of a complete catalog of space debris in the upper part of the low Earth orbits region (LEO). The purpose is to determine the achievable performances of a network of advanced optical sensors, through the use of the newest orbit determination algorithms developed by the Department of Mathematics of Pisa (DM). Such a network was designed and proposed to the European Space Agency (ESA) in the Space Situational Awareness (SSA) framework by Carlo Gavazzi Space SpA (CGS), Istituto Nazionale di Astrofisica (INAF), DM and Istituto di Scienza e Tecnologie dell'Informazione (ISTI-CNR).

The latest developed orbit determination algorithms were used to process simulated observations from the proposed network. In particular two innovative methods for preliminary orbit determination based on the first integrals of the Kepler problem were compared, by using them to process the same data. In both cases, the results showed that it is possible to use a network of optical sensors to build up a catalog containing more than 98% of the objects with perigee height between 1100 and 2000 km, and diameter greater than 8 cm. Such a catalog is obtained in just two months of observations. However, such results depend upon specific assumptions on the sensor and on the software technologies.

## **1. INTRODUCTION**

In the context of the European SSA program, the aim of the project SARA-Part I *Feasibility study of an innovative system for debris surveillance in LEO regime* was to demonstrate the feasibility of a European network based on optical sensors, capable of complementing the use of radars for the identification and cataloging of debris in the high part of the low Earth orbits (LEO) region, to lower the requirements on the radar system in terms of power and performances. The proposal relied on the definition of a wide-eye optical instrument able to work in high LEO zone and on the development of new orbit determination algorithms, suitable for the kind and amount of data coming from the surveys targeting at LEOs.

A realistic simulation was performed [5,12], taking into account all the relevant elements of the optic system: the telescope design, the network of sensors, the observation constraints and strategy, the image processing techniques. Calo Gavazzi Space SpA (CGS) provided us with simulated observations, which were produced starting from the ESA-MASTER2005 population model, taking into account an advanced design for the optical sensors. These data were processed with innovative orbit determination algorithms to build-up a catalog from scratch. More than 98% of the objects with perigee height between 1100 and 2000 km, and diameter greater than 8 cm, were cataloged within two months of survey.

One of the key tools for the success of the SARA-Part I study was an innovative orbit determination algorithm, based on the first integrals of the Kepler problem, see [9,6]. Standard methods, such as Gauss' [8], require at least three observations per pass in order to compute a preliminary orbit, while the proposed algorithm needs only two exposures, observed at different passes. This results in a significant reduction of the number of required telescopes, thus of the cost of the entire system. In addition, the proposed method takes into account the nodal precession due to the quadrupole term of the Earth geopotential. Because of the low altitude of the orbits and the availability of only

one exposure per pass, this effect is not negligible and it must be considered since the first step of preliminary orbit computation.

After the conclusion of the SARA-Part I study, another method was developed for preliminary orbit computation, also based on the Keplerian integrals [10]. Its main advantage with respect to its predecessor is to require less computational power. The same data provided for the SARA-Part I study were processed with the new algorithm, with the aim to validate it, to verify its efficiency and to investigate the possible advantages coming from its use.

## 2. NETWORK DEFINITION AND ASSUMED TECHNOLOGY

In this section we summarize the considerations which led to the definition of a suitable network of optical sensors, as it was proposed in the SARA-Part I study. We recall also the assumed properties of the optical sensors, whose design is currently under study, and finally the assumptions on the available software.

To observe debris some conditions must be verified, which are dependent on the object orbit parameters, the observatory location and the seasonal factors. The first limitations derive from geometrical constraints. An orbiting object at a fixed altitude is visible only up to a given distance from a station, beyond which the object is under the minimum needed elevation, typically 15 deg. An high LEO has, on average, 4 passes/day above the required elevation, when observed from a station at low latitudes (within 30 deg). Note that these constraints apply also to a radar sensor. The main difference with radar arises because of the geometry of sunlight. For optical observations the ground station must be in darkness, with the Sun at least 10-12 deg below the horizon, so that the sky is dark enough to begin operations. This happens on average about 30-60 min after sunset and before sunrise, but it strongly depends on the latitude and the season of the station. Moreover, the orbiting object must be in sunlight, out of the shadow cone of the Earth, and the atmosphere must be clear, without dense clouds and light pollution.

Fig. 1 shows the shadow cone for a nearly tropical station (latitude 27 N), on March 20th, at the local solar time 19 h. The red line represents the boundary of Earth shadow at 1400 km above the ground. The Earth shadow region is grey. The circles represent the iso-elevation directions of the sky above the horizon of the location, which is represented by the outer circle. The centre of the plot is the local zenith. The labelled lines (30, 60, 90 and 120) represent the iso-phase curves for objects at 1400 km above the ground; the apparent magnitude of the objects strongly depends upon the phase, e. g., a phase of 90 deg results in an increase by more than 3 magnitudes with respect to phase 0. The plot shows that the regions with smaller phase angles are the ones close to the Earth shadow boundary. The best conditions to observe objects at the smallest possible phase angles are during the minutes just after sunset or before sunrise, when the shadow region is smaller. Very small objects, down to some centimetres, are detectable only when they are very close to the Earth shadow boundary and during the short observability window either after sunset or before sunrise.

The meteorological constraints can be handled by having stations far enough to have low meteorological correlation. An high inclination object is more likely to be observed by an high latitude station. To guarantee a good coverage in all seasons both North and South high latitude stations are required. By drawing a shadow cone figure like Fig. 1, it is easy to see that the larger is the latitude, the smaller is the obstruction to observability due to the Earth shadow. However, an higher latitude implies shorter hours of darkness in summer and bad weather in winter, thus intermediate latitude stations, around 45 deg, are the best compromise. The network needs to be spread over the world to increase the efficiency of the system, but there are geopolitical and logistic constraints to be considered: availability to Europe, orography, electrical power, airports, and so on. The optical station network devised for our simulations was made of 7 stations: 3 in the equatorial area, which are Teide (Canary islands), Hao (French Polynesia) and New Norcia (Australia); 2 in the Northern hemisphere, which are Gran Sasso (Italy) and Pico de Vara (Azores); 2 in the Southern hemisphere, which are Falkland Islands and Malargue (Argentina). The network was chosen using the information on the meteorological conditions, simulated on the basis of the actual public-domain weather satellite data, mainly from the ISCCP (NASA) project (<http://isccp.giss.nasa.gov/index.html>).

We assumed a large field telescope based upon a Fly-Eye technology, whose architecture and design is under study in the European Space Agency (ESA) program denominated *CO-V Telescopes Analysis and Design*, see [4]. The telescope has a primary mirror of 110 cm diameter, with equivalent aperture of 100 cm, and it has the capability of fast motion. The field of view covers 45 deg<sup>2</sup>. The telescope is adequate to perform both survey and follow-up

observations. Moreover, the “idle time” in LEO observations due to the Earth shadow can be exploited to observe objects in higher orbits with only software changes, typically with longer exposures, from 10 to 60 s.

A very tricky problem of advanced sky surveys is the fill factor, which is the ratio between the active portion of the focal plane and its total area. The assumed Fly-Eye telescope has the cameras well separated with a private focal plane segment for each one, resulting in a correlated fill factor exactly 1. Moreover, commercial chips with fill factor greater than 0.99 are available, thus we could avoid to consider the fill factor in the simulation, by assuming it very close to 1. Each pixel of the CCD sensors corresponds to 1.5 x 1.5 arcsec on the celestial sphere, thus an image has 256 Megapixels.

Another assumption concerns the image processing software. Instead of being based upon the identification of the individual pixels with high enough signal to noise ratio S/N, it is thought to specifically detect trailed images, by summing the readings along all possible lines in the frame, thus allowing to detect trails with S/N on each pixel even less than 1. Algorithms with this capability exist, have acceptable computational complexity and have been tested [13]. The actual implementation in operational software and field testing is an assumption. We assumed also to be able to reduce astrometrically the observations in an accurate way, with RMS error of 0.4 arcsec when the pixel S/N is good. When the RMS grows to more than 2 arcsec, see (3) below, orbit determination failure can occur.

A very critical observing parameter for a debris is the phase angle. To our knowledge, there is no calibration of the magnitude dimming due to the phase angle for space debris, while there is such a function for asteroids [3]. In our simulations the official IAU magnitude system, called H-G system, was used. We assumed a scheduler capable of taking into account the geometry of light and the phase, chasing the lowest possible phase out of the Earth shadow.

### 3. POPULATION MODEL

In order to produce a realistic simulation of the whole observation process a suitable population of orbiting objects is required. A subset of the ESA-MASTER2005 population, upgraded with the recent in-orbit collisions (FengYun-1C, IRIDIUM 33 - COSMOS 2251) was provided by the European Space Operation Centre (ESOC). The MASTER model contains the largest objects taken from the USSTRATCOM Two Line Elements plus smaller objects generated with ad hoc source models. The population file did not contain any value for the albedo of the objects, a quantity that is needed to derive the magnitude of the object in the sky. From the available literature [1,11], a commonly accepted value of the albedo for a generic spacecraft is between 0.1 and 0.2. Therefore we made the conservative assumption of albedo 0.1 for all the objects. The absolute magnitude was derived according to the IAU standard for asteroids. The formula is  $H = 33 - 5 \log_{10}(d)$ , where  $d$  is the diameter of the object in m, provided by the MASTER file.

### 4. SNR MODEL

For each simulated observation the signal to noise ratio S/N expected at the observatory station performing the observation was computed, according to the following statistical model. Equations (2) are the formulas used for the computation of the S/N respectively for a starry source, a single pixel and an entire trail:

$$\frac{S}{N}_{star} = \frac{S}{\sqrt{S+N}}; \quad \frac{S}{N}_{pixel} = \frac{S/T}{\sqrt{S/T+N}}; \quad \frac{S}{N}_{trail} = \frac{S}{\sqrt{S+NT}}, \quad (2)$$

where  $T$  is the number of pixels trailed in the camera field during the exposure time. In this expressions  $N$  includes all the contributions from the sources of noise: the readout noise, the dark current noise and the sky background; the other term under square root accounts for the Poisson statistics. The expected signal is determined as a function of the object apparent magnitude, given the instrumental and observation parameters. The S/N for a single pixel is given by dividing the total signal of the debris by  $T$ . In this context,  $N$  is the noise in a single pixel, while in the formula for a star  $N$  is spread in few pixels, depending on the point spread function of the starry object. The algorithm described in [13] is capable to detect very faint trails, thanks to its capability of adding the signal along the trail direction. The resulting S/N formula for the entire trail is obtained by adding the signal belonging to all the pixels of the trail. This gives a contribution in the noise proportional to  $T^{1/2}$ . We used  $S/N_{trail} \geq 6$  as a criterion for the detectability of a trail, in order to avoid false detections.

When the detected trail is too faint, the problem is to determine its beginning and end with high accuracy. In this case the astrometric error  $Z$  can be computed by

$$Z \frac{S}{N_{pixel}} \leq \sqrt{Z} \rightarrow Z = \left( \frac{1}{S/N_{pixel}} \right)^2. \quad (3)$$

In practice there are two regimes for the astrometric error. When the signal is strong, the astrometric error is dominated by the astrometry method, that is by the systematics in the astrometric catalogs. When the signal is weak, it is determined by (3).

Fig. 2 shows the curves of the S/N as function of the apparent magnitude for different cases. The blue line represents the case of a fixed star (no trailing), while the red lines correspond to a LEO object at 1400 km of altitude, respectively when the number of pixels  $T$  is minimum ( $T=200$ , solid red line) and when it is maximum ( $T=600$ , dashed red line). The plot also shows the degradation of the astrometric performance for low S/N on a single pixel, due to the difficulty of determining the beginning and end of the trail. The green line, representing the S/N over a single pixel when  $T=200$ , changes colour (green  $\rightarrow$  red) when the astrometric error, represented by the magenta line, becomes greater than 0.4 arcsec and it becomes black when the corresponding  $S/N_{trail}$  for  $T=200$  (solid red line) becomes lower than 6, in which case the object cannot be imaged in survey mode.

## 5. CORRELATION AND ORBIT DETERMINATION

Given two or more sets of observations, the main problem is to identify which separate data belong to the same object (correlation problem). Thus the orbit determination problem needs to be solved in two stages: first different observational data need to be correlated, then an orbit can be determined. The two Keplerian integrals methods, briefly described below, allow us to compute an orbit starting from only two exposures, taken at different passes, which can be distant in time up to 1 day or more, corresponding to several revolutions. Starting from scratch, without any a priori information on the observed objects, for any couple of exposures we must try to compute a preliminary orbit, solution of a 2-body approximation, or possibly taking into account the second zonal spherical harmonic of the Earth geopotential. This step has a computational cost growing with the square of the number of observed trails. This justifies the search for a method that requires the lowest possible computational power.

The preliminary orbits obtained with one of the Keplerian integrals methods have to be replaced in a later stage by least squares orbits, with a dynamical model including all the relevant perturbations. The accuracy of an orbit fitting with only two trails is very poor, due to the low information available, and in particular it can be false, indicating an unreal object. This can happen in two ways: one possibility is that the two trails belong to different objects, the other

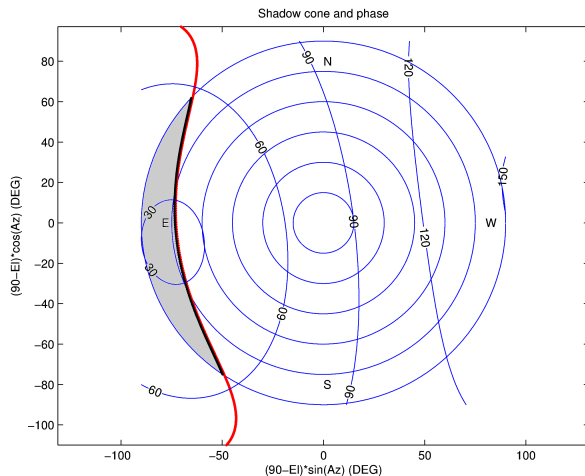


Fig. 1. Earth Shadow and iso-phase curves for a tropical station at local time 19 h on March 20th

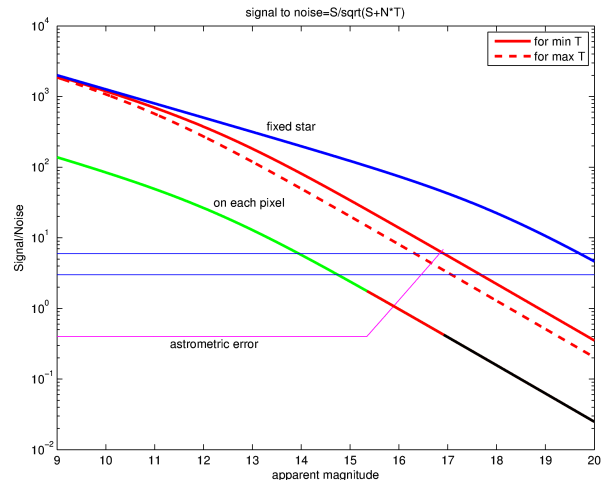


Fig. 2. Signal to noise ratio

one is that even if the trails really belong to the same object, the orbit is completely wrong, to a measure that it is not possible to correlate other trails of the same object. Thus 2-trails correlations needed to be confirmed by correlating further observations. This was done by the attribution procedure, which consists in trying to fit new observations to a known orbit, see [14, Sec. 7.6]. When an orbit is very well constrained and the number of involved trails is high enough, the possibility for the corresponding correlation to be false can be ruled out, by removing discordant correlations. We found empirically that the minimum number of trails required to exclude false correlations was 4. Thus, in our simulations we required at least 4 trails to accept an orbit and in this case the object was cataloged. When the number of fitting trails increased to 10, the object was numbered, by assigning a unique identifier (name).

The information related to a single object during an exposure can be summarized in an attributable, which is a 4-dimensional vector  $A=(\alpha,\delta,d\alpha/dt,d\delta/dt)$ , representing the angular position and velocity of the body at a time  $t$ . Usually  $\alpha, \delta$  are right ascension and declination. To compute a 6 parameters orbit, 2 further quantities, such as range and range rate ( $\rho, d\rho/dt$ ), are needed. In our two simulations we used the Keplerian integrals methods to produce preliminary orbits from two attributables  $A_1, A_2$  of the same object at two epoch times  $t_1$  and  $t_2$ . With the first method polynomial equations are derived from the constancy of angular momentum and energy. With the second one a suitable component of the Laplace-Lenz vector is used instead of the energy and this choice leads to a polynomial system of smaller degree, less than half of the other. In the following we recall both methods, which are named respectively energy method and Laplace-Lenz vector method.

The energy method is introduced in [9]. The 2-body energy  $E$  and the angular momentum  $\mathbf{c}$  can be expressed as functions of  $A, \rho, d\rho/dt$ . By assuming the orbit between  $t_1$  and  $t_2$  well approximated by a Keplerian one, we have

$$E(A_1, \rho_1, \dot{\rho}_1) - E(A_2, \rho_2, \dot{\rho}_2) = 0, \quad \mathbf{c}(A_1, \rho_1, \dot{\rho}_1) - \mathbf{c}(A_2, \rho_2, \dot{\rho}_2) = \mathbf{0}. \quad (4)$$

The above system can be reduced to a polynomial one in the two variables  $\rho_1, \rho_2$ , with total degree 48. By means of the resultant method from Computational Algebra, one of  $\rho_1, \rho_2$  is eliminated, thus getting a univariate polynomial of degree 48. All positive real roots are computed by means of an optimized algorithm [2], so that all the solutions of (4) are finally obtained. Since the degree of the system is very high, we need quadruple precision. By using the Keplerian approximation, compatibility conditions are imposed: the first one related to the perigee argument and the second one to the mean anomaly. The discrepancy from them is measured by a suitably defined norm  $\chi$ . If such  $\chi$  is smaller than a fixed threshold, the solution is accepted. The algorithm also provides a covariance matrix for the computed orbit. Typically less than 3 orbits remain after the entire procedure.

The Laplace-Lenz vector method is introduced in [10]. The Laplace-Lenz vector is the vector on the orbital plane of an Earth orbiting object whose direction points from the Earth center of mass to the position of perigee, and whose length is equal to the orbit eccentricity. In the two-body approximation it is a constant of motion. The Laplace-Lenz vector  $\mathbf{L}$  and the angular momentum  $\mathbf{c}$  can be expressed as functions of  $A, \rho, d\rho/dt$ . By assuming the orbit between  $t_1$  and  $t_2$  well approximated by a Keplerian one, we have that

$$(\mathbf{L}(A_1, \rho_1, \dot{\rho}_1) - \mathbf{L}(A_2, \rho_2, \dot{\rho}_2)) \cdot \mathbf{v} = 0, \quad \mathbf{c}(A_1, \rho_1, \dot{\rho}_1) - \mathbf{c}(A_2, \rho_2, \dot{\rho}_2) = \mathbf{0}, \quad (5)$$

where  $\mathbf{v}$  is a fixed direction, not parallel to the angular momentum  $\mathbf{c}$ , in order to have independent equations ( $\mathbf{L} \cdot \mathbf{c} = 0$ ). The above system can be reduced to a polynomial one in the two variables  $\rho_1, \rho_2$ , with total degree 20. By means of the resultant method, one of  $\rho_1, \rho_2$  is eliminated, thus getting a univariate polynomial of degree 20. All positive real roots are computed by means of the algorithm of [2], so that all the solutions of (5) are finally obtained, but in this case quadruple precision is not necessary and moreover it does not give any advantage. As in the other method, compatibility conditions are imposed, related to the perigee argument and the mean anomaly and the discrepancy from them is measured by a suitably defined norm  $\chi$ . If such  $\chi$  is smaller than a fixed threshold, the solution is accepted. Even in this case the algorithm provides a covariance matrix for the computed orbit and usually less than 3 orbits remain after the entire procedure.

To deal with LEOs it is necessary to generalize these methods, including the effect due to the Earth oblateness [6]. The secular equations for Delaunay's variables  $\ell, \omega, \Omega, L=(\mu a)^{1/2}, G=L(1-e^2)^{1/2}$  and  $Z=G \cos(I)$  are given by

$$\begin{aligned}\bar{\ell} &= n - \frac{3}{4} n \left( \frac{R_{Earth}}{a} \right)^2 \frac{J_2 (1 - 3 \cos^2(I))}{(1 - e^2)^{3/2}}, & \bar{\omega} &= \frac{3}{4} n \left( \frac{R_{Earth}}{a} \right)^2 \frac{J_2 (4 - 5 \sin^2(I))}{(1 - e^2)^2}, \\ \bar{\Omega} &= -\frac{3}{2} n \left( \frac{R_{Earth}}{a} \right)^2 \frac{J_2 \cos(I)}{(1 - e^2)^2}, & \bar{L} = \bar{G} = \bar{Z} &= 0,\end{aligned}\tag{6}$$

where  $J_2$  is the coefficient of the second zonal spherical harmonic of the Earth gravity field,  $\ell$  is the mean anomaly,  $\omega$  is the perigee argument,  $\Omega$  is the longitude of the ascending node,  $\mu$  is the standard gravitational parameter of the Earth,  $a$  is the semimajor axis,  $e$  is the eccentricity,  $I$  is the inclination and  $n = \mu a^{-3/2}$  is the mean motion. In this case we cannot use the conservation of angular momentum, since it precedes: for example, for a typical LEO object orbiting at 1400 km of altitude the velocity of precession is  $5 \cos(I)$  deg/day. Even the Laplace-Lenz vector is not constant. Thus we consider the parametric problem obtained by imposing  $d\Omega/dt = K_1$ ,  $d\omega/dt = K_2$ ,  $d\ell/dt = K_3$  with  $K_1, K_2, K_3$  constants. We obtain systems (7) and (8) respectively for the energy and the Laplace-Lenz vector methods:

$$E(A_1, \rho_1, \dot{\rho}_1) - E(A_2, \rho_2, \dot{\rho}_2) = 0, \quad R_c \mathbf{c}(A_1, \rho_1, \dot{\rho}_1) - \mathbf{c}(A_2, \rho_2, \dot{\rho}_2) = 0,\tag{7}$$

$$(R_L \mathbf{L}(A_1, \rho_1, \dot{\rho}_1) - \mathbf{L}(A_2, \rho_2, \dot{\rho}_2)) \cdot \mathbf{v} = 0, \quad R_c \mathbf{c}(A_1, \rho_1, \dot{\rho}_1) - \mathbf{c}(A_2, \rho_2, \dot{\rho}_2) = 0,\tag{8}$$

where  $R_c$  is the rotation by  $\Delta\Omega = K_1(t_2 - t_1)$  around the vertical axis, and  $R_L = R_2 R_c R_1$ , with  $R_1$  the rotation by  $-\omega_1$  around the direction of  $\mathbf{c}_1 = \mathbf{c}(A_1, \rho_1, d\rho_1/dt)$ ,  $R_2$  the rotation by  $\omega_2 + K_2(t_2 - t_1)$  around the direction of  $\mathbf{c}_2 = \mathbf{c}(A_2, \rho_2, d\rho_2/dt)$ . Thus, given fixed values of  $K_1, K_2, K_3$  and the rotation matrices  $R_c$  and  $R_L$ , the problem has the same algebraic structure of the unperturbed one. The compatibility conditions contain the perigee precession and the secular perturbation in mean anomaly, expressed by the constants  $K_2, K_3$ . The covariance matrix can be computed as well.

To solve the obtained parametric system (7) or (8), we set up a fixed point iterative procedure as follows. First, we solve it for  $K_1 = K_{01}, K_2 = K_{02}, K_3 = K_{03}$ , by selecting the values  $K_{01}, K_{02}, K_{03}$  and the corresponding rotation matrices  $R_c$  and  $R_L$ , either using the circular orbits corresponding to each of the two attributables [7] or by assuming  $K_{01} = K_{02} = K_{03} = 0$ . Among the obtained solutions, we cannot know which one could lead to convergence. Since the values of  $K_{01}, K_{02}, K_{03}$  are quite arbitrary, it is not safe to select only those with a low value of  $\chi$ . Thus we use all the solutions as possible starting guess for the iterative procedure. Given the orbital elements  $E_i$  at step  $i$  we compute new values for  $K_1, K_2, K_3$  by (6) and the new rotation matrices  $R_c$  and  $R_L$ , and for them we solve the corresponding parametric system. We select the solution with the lowest value of  $\chi$  and compute the corresponding orbital elements  $E_{i+1}$ . Then we keep iterating until convergence.

## 6. CATALOG BUILD-UP SIMULATIONS

Our aim was to validate the latest developed Laplace-Lenz vector algorithm and make a comparison with the energy method, successfully tested in the SARA-Part I study, in order to establish the pros and cons of it. Therefore the same data provided for the SARA-Part I study were processed again, by using both methods in two independent simulations. The entire procedure for the catalog build-up was essentially the same as in the SARA-Part I study for both simulations. The only difference was in the computation of preliminary orbits from two attributables, when the Laplace-Lenz vector method was used. Actually, there were also other minor differences, coming from improvements in different parts of our orbit determination software, which were unavoidably involved. Then we needed to run again also the simulation with the energy method, to be sure to make the comparison in the right way.

We assumed to start with no information on the satellite and debris population in the region of interest (high LEO) and attempted to build up an orbit catalog, to be compared with the MASTER one. We conducted a large scale simulation, by choosing two different population samples, dubbed Population 1 and Population 2. Population 1 was made up of 912 objects, randomly selected among those with diameter between 8 and 27 cm, and with altitude of perigee  $h_p$  between 1300 and 2000 km. Population 2 included 1104 objects, with diameter between 5 and 25 cm, and with  $1000 \leq h_p < 1300$  km. Objects larger than 27 cm and 25 cm respectively were not included in the simulation: as showed in the SARA-Part I study, the amount of observational data for these objects is so large to allow us to attain

a complete catalog within 1 month. This is confirmed also with the Laplace-Lenz vector method, as will be clear after the analysis of the results.

In the MASTER population model, smaller objects typically are sampled, i. e. a single object represents many fragments. Simple de-sampling (e. g. by assigning different mean anomalies to each fragment, keeping all the other orbital elements the same) could affect our simulations by generating false correlations. Therefore the sampled fragments were treated as single objects in the simulation process. A *sampling factor* was associated to each object to represent the number of fragments within the same orbit in the final analysis of the results.

A first qualitative analysis of the results can be done through Fig. 3 and Fig. 4, which show the outcome of the catalog build-up on the perigee altitude-diameter plane, respectively when the Laplace-Lenz vector method and when the energy method was used. The results are obtained starting from the same simulated observations, which cover two months of survey. The two rectangles enclose the regions corresponding to the selected population samples. The parabolic curves represent two possible radar performances in the case of a baseline radar (dashed line) and of an enhanced one (solid line), to be used along with the optical sensors in the ESA-SSA program. The corresponding assumptions on the radar systems are rather arbitrary, thus this performance curves have to be considered just as a comparison benchmark: indeed, the purpose of the investigation was to determine the requirement for a future radar system, and to see how much this could change by assuming the cooperation of a network of optical sensors. These curves give the minimum diameter  $d_{\min}$  of observable objects as function of the perigee altitude  $h_p$ , according to  $d_{\min} = (h_p/h_{\text{ref}})^2 d_{\text{ref}}$ , where  $h_{\text{ref}}$  and  $d_{\text{ref}}$  are reference values for the perigee altitude and the diameter. This equation is a simple consequence of the inverse fourth power dependence of radar S/N from distance. We set  $h_{\text{ref}} = 2000$  km and  $d_{\text{ref}} = 32$  cm for the baseline radar, as presently foreseen by the European SSA system. For the enhanced radar we took  $h_{\text{ref}} = 2000$  km and  $d_{\text{ref}} = 20$  cm. The two rectangles cover the region lying above the curve of the enhanced radar. The results for both the population samples after 2 months of survey observations are reported. Resident LEOs are represented by points, objects in orbits transiting in the LEO region by circles. The green color means that the overall procedure succeeded in obtaining an orbit for the object, red that there were no observations and black that the observations did not suffice to obtain an acceptable orbit. The reasons for the occurrence of this last possibility are essentially two: the observations were very few and too distant in time, so that correlation was not possible; the observations had low accuracy, so that both the computation of an orbit or the attribution of further trails failed.

The two figures are very similar, except for few more black circles (exactly 10 over a total of 206 circles) and dots (25 over 1810) for the simulation which uses the Laplace-Lenz vector method (Fig. 3). Anyway, the presence of black and red dots is relevant only in the low region of Population 2 for both the simulations. This means that, in the case of resident LEOs, the failure of catalog build-up can happen only for some fast moving objects with diameter smaller than 8 cm. Moreover, the outcome of the two simulations suggests that the problem is not the altitude but the

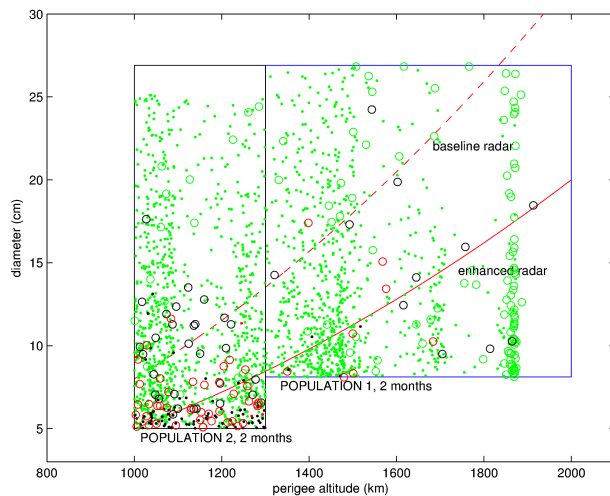


Fig 3: Results after two months of survey with the Laplace-Lenz vector method.

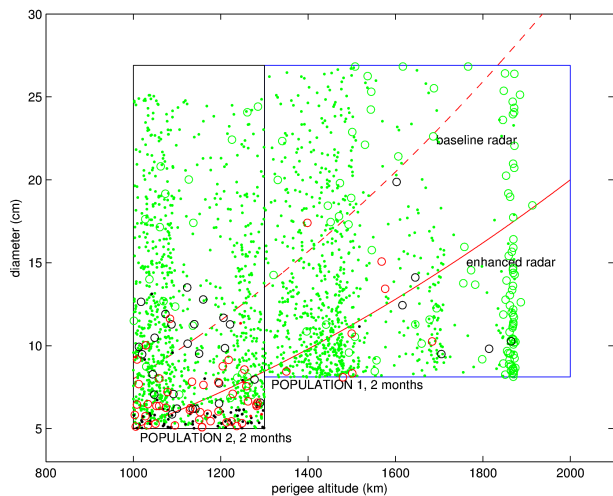


Fig 4: Results after two months of survey with the energy method.

diameter. We can see from the figures that for the objects larger than 8 cm there are problems only if they are on very eccentric transit orbits, but almost all resident LEOs are cataloged. Smaller debris instead require a larger telescope, whatever the height. Moreover, the figures show that most of the difficulties in the catalog build-up concern the region of orbital perigee altitude less than about 1100 km.

## 7. ANALYSIS OF THE RESULTS

To analyze the results, we measured the efficiency of the catalog build-up, defined as the ratio between the number of reliable orbits computed (with at least 4 trails) and the total number of sampled objects. We measured also the efficiency relative to objects lying in the region of the perigee altitude-diameter plane above the curve of the enhanced radar, and finally that for objects with diameter greater than 8 cm. These quantities were computed accounting for the number of clones for the sampled objects (sampling factor), to count both the successes and the failures of correlation.

The results for Population 1 were overwhelming for both methods, even if the efficiency of the Laplace-Lenz vector method was slightly lower. For  $h_p \geq 1300$  km, we computed the orbits of almost all the objects above 8 cm: 98.4% with the energy method and 97.5% with the Laplace-Lenz vector method. If we consider only resident LEOs the percentages are 99.9% and 99.5% respectively. By restricting to the objects above the curve of enhanced radar performance of Fig. 3 and Fig. 4, the total efficiencies are respectively 99.0% and 97.8%, while for resident LEOs they are 100% and 99.8%. With both methods there were problems for objects in highly eccentric transit orbits (e. g. GTO): half of them was never observed and for more than a half the trails were less than 4, so that it was impossible to catalog them (we accepted an orbit only when the fitting trails were at least 4). Anyway, these objects should be observed with a different strategy, such as non-sidereal tracking targeting them at apogee [15].

For Population 2 the total efficiencies are 84.2% with the energy method and 79.8% with the other one. In this case the difference between the two methods is more evident, as we can see also by comparing Fig. 3 and Fig. 4. If we restrict to resident LEOs the efficiencies are respectively 88.1% and 83.8%. If we take into account only the region above the curve of the enhanced radar the difference is smaller: the overall efficiencies are 92.8% for the energy method and 89.5% for the other one. For resident LEOs the efficiencies are respectively 96.4% and 93.2%. As already pointed out, the problem for our optic system is not the perigee height but the object diameter: if we take into account only the objects with diameter greater than 8 cm, then the efficiencies grow to 96.0% with the energy method and 95.3% with the other one. For LEOs the percentages are very high: 99.1% and 98.8% respectively.

To get the big picture of the results, we should take into account also the biggest objects of the MASTER population. Moreover, the results for Population 1 have to be weighted twice, since we randomly selected only half of the objects with the same range for perigee altitude and diameter. We can infer from the results of our simulations (see Fig. 3 and Fig. 4) that all the objects of the MASTER population with perigee altitude between 1000 km and 2000 km, which have diameter greater than 25 cm can be cataloged within two months, as a consequence of the abundance of observations. Actually in our simulations all the objects with diameter greater than 22 cm were already cataloged within the first month, except for one object on a very eccentric orbit (eccentricity 0.7) with diameter equal to 24.2 cm. Then, assuming that all the biggest objects of the MASTER population not contained in our population samples, with perigee altitude between 1000 km and 2000 km, were cataloged within 2 months of survey, the overall efficiencies relative to the objects above the enhanced radar curve are 98.0% for the energy method and 96.9% for the Laplace-Lenz vector method. But if we consider the objects with diameter greater than 8 cm, regardless of the perigee height, the percentages become 98.8% and 98.3%. As noted in section 6, most of the difficulties arise for the region of orbital perigee altitude less than 1100 km and, on the other hand, only the dimension of the objects is relevant for the efficiency. If we discard the region of perigee altitude less than 1100 km and consider only objects with diameter greater than 8 cm, the total efficiencies are 98.9% and 98.5% respectively for the energy and the Laplace-Lenz vector method. By considering only resident LEOs they are 99.9% and 99.7%.

From the analysis of the efficiencies reached with the two methods we see that the energy method gives a slight advantage. A disadvantage of this method comes from the high degree of the polynomial system to be solved, which implies the need for quadruple precision to obtain the right solutions. Then the computational cost of any single step of the algorithm which compute preliminary orbits from any couple of trails is quite high and, since the cost grows as the square of the number of trails, the computing time can easily become relevant. With the Laplace-Lenz vector method, the computational cost strongly decrease, since quadruple precision is no more necessary. Some preliminary

tests showed that the routine implementing the Laplace-Lenz vector method for the computation of preliminary orbits is 100 times faster than the one using energy.

In our simulations the data were processed day by day. The overall procedure was parallelized and 24 cores were used for each simulation. For any batch of trails to be processed, there are two steps to be performed: the correlation of the new trails to already cataloged orbits and then the computation of new orbits from the left uncorrelated trails. To have a measure of the possible gain in CPU time attainable with the Laplace-Lenz vector method, we considered only the CPU times of the second step for each day of observations. This step includes not only the computation of preliminary orbits, but also the differential corrections, the attribution of other trails from the same batch, and finally the *correlation management* to eliminate duplicates and discordant correlations.

At the beginning of the first day the catalog was empty, then the difference between the two methods was more appreciable. For Population 1, the trails of the first day were 2496. With the energy method our software took 413 minutes to process these data, while with the Laplace-Lenz vector method it took only 23 minutes, about 18 times less. For the entire simulation, covering 2 months of observations, the total number of trails was 113396. By considering only the second step of each day of data processing, the total CPU time was 1352 minutes with the energy method, while it was 234 minutes with the other one, about 6 times less. The CPU times for the entire procedure were respectively 2956 minutes with the energy method and 1810 minutes with the Laplace-Lenz vector method, almost 2 times less. For Population 2 the results are similar. For the first day the trails were 1997. The CPU times to process them were 256 against 13 minutes, with a ratio of about 20. For the entire period of two months the trails were 90510. By considering only the second step of the procedure for each day, the CPU times were 3119 and 551 minutes respectively for the energy method and the Laplace-Lenz vector method, with a ratio of about 6. The CPU times for the entire simulations were respectively 4838 minutes with the energy method and 2239 minutes with the Laplace-Lenz vector method, more than 2 times less.

A deeper analysis shows that a marked difference between the two methods is appreciable only during the first days of catalog build-up. Indeed, our simulations start to construct the catalog from scratch, with no previous information on the objects observed. Thus, during the first day of survey we can observe a peak in the CPU time spent by the energy method to try to correlate all the possible couples of trails, corresponding to thousands of observations. When dealing with the entire population of high LEOs, this phase requires either a very fast algorithm or very powerful hardware, that is no more needed after some days of catalog build-up, when the catalog is rich enough to allow the correlation of most of the trails to already cataloged orbits. With the Laplace-Lenz vector method the peak of CPU time of the first days disappears, thus the problem to face the high computational cost of a cold start is solved and there is no waste of technology.

The conclusion is that an ad hoc combination of the two methods is the best compromise. The Laplace-Lenz vector method should be used to start the construction of the catalog. After a week of catalog build-up, the daily process of the data can be performed with one of the two methods equally, for example the Laplace-Lenz vector one. Then the other method can be employed periodically, e. g. once a week, to process the left uncorrelated trails, in order to catalog the highest possible number of objects. In this way we can reach the best results from the point of view of both the efficiency and the processing time. It must also be stressed that both the algorithms can be further optimized and that even the parallelization procedure can be improved. We are working on that.

## 8. POSSIBILITY OF FOLLOW-UP

In section 2 we stressed the possibility of the assumed fly-eye telescope to perform follow-up. Then we would like to verify if the obtained orbits are accurate enough to give us such a possibility. Tasking observations are possible if, by moving the telescope at non-sidereal rate, the object remains in the telescope field of view. Moreover, it is desirable to see the object with most signal concentrated on a single pixel, thus obtaining a higher signal with respect to the survey mode. We considered the numbered objects obtained after 1 month and we propagated the orbits for 1 week after the last observation. Then the angular error in prediction and the relative error in angular velocity were computed. Taking into account that the angular velocity of the objects in our sample was less than 2000 arcsec/s, to see the object in a single pixel during tasking the relative error in angular velocity had to be less than  $7.5 \times 10^{-4}$ . This was achieved for all the numbered objects with both methods. Moreover the angular error in position was always less than 121 arcsec. Then the possibility of follow-up is confirmed and moreover tasking observations are possible without trailing loss.

## 9. CONCLUSIONS

The results of the two catalog build-up simulations show that more than 98% of the LEO objects with perigee height above 1100 km and diameter greater than 8 cm can be cataloged in 2 months, by using orbit determination methods based on the Keplerian integrals. As Fig. 3 and Fig. 4 shows, a central area around 1100 km of orbital perigee altitude has been identified where the radar and the optical network should operate in a cooperative way. All the numbered orbits are accurate enough to allow follow-up observations with no trailing loss, to be processed in the orbit improvement phase, with the aim to obtain orbits accurate enough to be used for collision avoidance. All of this is a consequence of the assumed technology, which includes a suitably defined network of innovative optical sensors, the Fly-Eye telescopes, as well as advanced software both for image processing and orbit determination.

## 10. ACKNOWLEDGEMENTS

We wish to thank CGS for providing us with the expected sensor performances and realistic simulated observations, taking into account the characteristics of the Fly-Eye telescope, the meteorological model to account for cloud cover, and the statistical model for the signal to noise ratio. This work was conducted partially under ESA/ESOC contract 22750/09/D/HK SARA-Part I *Feasibility study of an innovative system for debris surveillance in LEO regime*, with CGS as prime contractor.

## 11. REFERENCES

- [1] J.L. Africano, E.G. Stansbery, and P.W. Kervin, "The optical orbital debris measurement program at NASA and AMOS," *Advances in Space Research*, vol. 34/5, pp. 892-900, 2004.
- [2] D.A. Bini, "Numerical computation of polynomial zeros by means of Aberth method," *Numerical Algorithms*, vol. 13/3-4, pp. 179-200, 1997.
- [3] E. Bowell, B. Hapke, D. Domingue, K. Lumme, J. Peltoniemi, and A.W. Harris, "Application of photometric models to asteroids," *Asteroids II*, The University of Arizona Press, 1989.
- [4] L. Cibirin, M. Chiarini, A. Bertoli, F. Villa, L. Dimare, D. Farnocchia, F. Bernardi, A. Milani, G.M. Pinna, I. Zayer, P.M. Besso, R. Ragazzoni, and A. Rossi "A dynamic observation concept as a key point for an enhanced SSA optical network", *Proceedings of the European Space Surveillance Conference WPP-321, 7-9 June 2011, Madrid, Spain*.
- [5] L. Dimare, A. Milani, D. Farnocchia, A. Rossi, and F. Bernardi, "Innovative orbit determination algorithms for a complete Debris catalog in the upper LEO region," *Proceedings of the European Space Surveillance Conference WPP-321, 7-9 June 2011, Madrid, Spain*.
- [6] D. Farnocchia, G. Tommei, A. Milani, and A. Rossi, "Innovative methods of correlation and orbit determination for space debris," *Celest. Mech. Dyn. Astr.*, vol. 107/1-2, pp. 169-185, 2010.
- [7] K. Fujimoto, J.D. Maruskin, and D.J. Scheeres, "Circular and zero-inclination solutions for optical observations of Earth-orbiting objects," *Celest. Mech. Dyn. Astr.*, vol. 106, pp. 157-182, 2010.
- [8] K.F. Gauss, *Teoria motvs corporvm coelestivm in sectionibvs conicis solem ambientivm*, Hambvrgi, Svmtibvs F. Perthes et I.H. Besser, 1809.
- [9] G.F. Gronchi, L. Dimare, and A. Milani, "Orbit determination with the two-body integrals," *Celest. Mech. Dyn. Astr.*, vol. 107/3, pp. 299-318, 2010.
- [10] G.F. Gronchi, D. Farnocchia, and L. Dimare, "Orbit determination with the two-body integrals II," *Celest. Mech. Dyn. Astr.*, vol. 110/3, pp. 257-270, 2011.
- [11] D.J. Kessler, and K.S. Jarvis, "Obtaining the properly weighted average albedo of orbital debris from optical and radar data," *Advances in Space Research*, vol. 34/5, pp. 1006-1012, 2004.
- [12] A. Milani, D. Farnocchia, L. Dimare, A. Rossi, F. Bernardi, "Innovative observing strategy and orbit determination for Low Earth Orbit Space Debris," submitted.
- [13] A. Milani, A. Villani, and M. Stiavelli, "Discovery of very small asteroids by automated trail detection," *Earth, Moon, and Planets*, vol. 72, pp. 257-262, 1996.
- [14] A. Milani, and G.F. Gronchi, *Theory of orbit determination*, Cambridge University Press, 2010.
- [15] A. Milani, G. Tommei, D. Farnocchia, A. Rossi, T. Schildknecht, and R. Jehn, "Orbit determination of space objects based on sparse optical data," *MNRAS*, in press.